A. Calloni, A. Dupasquier, R. Ferragut, P. Folegati, M. M. Iglesias, I. Makkonen, and M. J. Puska, Positron localization effects on the Doppler broadening of the annihilation line: Aluminum as a case study, Physical Review B 72, 054112: 1-6 (2005).

Positron localization effects on the Doppler broadening of the annihilation line: Aluminum as a case study

A. Calloni, A. Dupasquier, R. Ferragut, P. Folegati, and M. M. Iglesias
Dipartimento di Fisica e Centro L-NESS, Politecnico di Milano, Via Anzani 52, 22100 Como, Italy

I. Makkonen and M. J. Puska
Laboratory of Physics, Helsinki University of Technology, P.O. Box 1100, FIN-02015 HUT, Finland
(Received 18 February 2005; revised manuscript received 20 June 2005; published 5 August 2005)

The coincidence Doppler broadening (CDB) technique is widely used to measure one-dimensional momentum distributions of annihilation photons, with the aim of obtaining information on the chemical environment of open-volume defects. However, the quantitative analysis of CDB spectra needs to include also purely geometrical effects. A demonstration is given here, on the basis of CDB spectra measured in quenched and in deformed pure aluminum. The comparison of the experimental results with *ab initio* computations shows that the observed differences come from the difference in free volume seen by positrons trapped in quenched-in vacancies or in vacancylike defects associated to dislocations. The computation reproduces accurately all details of CDB spectra, including the peak near the Fermi break, which is due to the zero-point motion of the confined positron.

DOI: 10.1103/PhysRevB.72.054112 PACS number(s): 78.70.Bj, 81.40.Ef

I. INTRODUCTION

Positron annihilation spectroscopy (PAS) is a well-established technique for lattice defect detection and for the experimental study of many defect-related phenomena, which has been discussed in various papers and textbooks (see, for instance, Refs. 1–3). It may be recalled that this technique is based on the ability of open volumes (vacancies and vacancy clusters, nanovoids, misfit surfaces) and of negatively charged defects to trap positrons. Positron trapping may be detected through three different symptoms: (i) reduction of the average distance traveled by a thermal positron (diffusion length L_+); also, in case of trapping at open-volume defects: (ii) reduction of the annihilation rate (reciprocal of the mean life τ); (iii) changes in the momentum distribution of the annihilation radiation. A different experimental approach to defect detection corresponds to each of the above effects; each method has its own merits that do not need to be discussed here, except to say that one special advantage of detecting the effects of trapping by measuring the momentum distribution of the annihilation radiation is the sensitivity to the chemical environment of the positron trap displayed in the high-momentum region. This circumstance enables one to study the association of vacancies with the different chemical species that may be present in a sample. The most frequent application of the method is based on the measurement of the Doppler broadening of the annihilation radiation, which reflects the motion of annihilating electron-positron pairs as seen in the laboratory reference frame. Since the fingerprint of the chemical species is given only by the small percentage of annihilation with fast electrons in nearly atomic energy bands, the momentum spectrum needs to be measured with very low background (about 10^{-5} times peak counts); this can be achieved by means of the coincidence Doppler broadening (CDB) technique, which implies the use of two gamma spectrometers to detect both annihilation photons in coincidence.[4]

Widespread use of the CDB technique for current defect studies in different kinds of materials (see, for instance, Ref. 5 for semiconductors and Ref. 6 for metal alloys) suggests discussing in detail the effects of positron trapping on the momentum distribution from a different viewpoint than adopted in the papers that have previously addressed this subject, which were mainly focused on the interpretation of the angular correlation of the annihilation radiation (ACAR). Pioneer ACAR work on defected materials is in Ref. 7; more recent results can be found in Refs. 8–13.

The most evident effects of positron localization in vacancies on momentum distributions are the reduction of the characteristic anisotropy related to the lattice symmetry and the enhancement of the distribution in the low-momentum region. A further effect, which is more easily seen in metals than in dielectrics, is given by the contribution of the positron to the total momentum of the e^+-e^- pair: when a positron moves freely at thermal energies in a crystal, this contribution is negligible, but it need not be so when the positron is spatially confined. As it was already realized by Shulmann and Berko,[14] the quantum confinement of the positron in a metallic environment manifests itself as a smearing of the Fermi break in the electron-positron joint momentum distribution. When CDB data are analyzed by taking ratios between different spectra, this smearing can originate very sharp structures, which need not be confused with other structures possibly due to chemical decoration of vacancies or to anisotropy in bulk spectra.

The present paper addresses the effects of positron confinement in CDB measurements on metals by discussing, as a case study, positron trapping at vacancies and vacancylike defects associated to dislocations in pure aluminum. The difference sensed by positrons between thermally generated vacancies and traps associated to dislocations is essentially the dimension of the open volume available for localization. Thus the choice of studying two slightly different species of

defects gives the possibility to explore the effects of changing the confinement volume. Experimental CDB data are presented and discussed below in combination with *ab initio* computations of one-dimensional momentum distributions.

II. EXPERIMENT

Two-dimensional energy spectra where measured by using two hyperpure Ge gamma spectrometers ($\sim$50% of relative efficiency for the ^{60}Co line at 1.33 MeV) coupled to a multiparameter acquisition system. The one-dimensional momentum spectrum $\rho(p_x)$ was obtained by summing the counts in the two-dimensional spectrum $S(E_1,E_2)$ along the line $p_x=(E_1-E_2)/c$ in the interval 1022 keV$-\Delta E<E_1+E_2<1022$ keV$+\Delta E$, where $\Delta E=2.1$ keV. The momentum resolution [$3.5\times10^{-3}\ m_0c$ for the full width at half maximum (FWHM) of the Gaussian resolution curve] was evaluated from the Doppler-free one-dimensional energy spectrum that one obtains by summing $S(E_1,E_2)$ along the lines $E_1+E_2=$const.

The ^{22}Na positron source was sandwiched between two Kapton foils (7.5 μm thickness). The fraction of annihilation in Kapton (12.5%) was determined by taking a lifetime spectrum for annealed Al. This fraction was assumed for subtracting the Kapton component in all CDB spectra; the shape of the Kapton CDB spectrum was determined in a separate experiment by using a thick Kapton sample.

The study of thermally generated vacancies was performed on 5–9-purity Al single crystals. The samples were heated at 417 °C, then quenched in water, rinsed in alcohol, dried with paper tissue, mounted with the positron source in the standard sandwich geometry and brought at liquid-nitrogen temperature (LNT). The whole procedure was completed in about 100 s. The measurements were taken at LNT. The momentum density distribution Δ as a function of the momentum p_x is presented in Fig. 1(a) without smoothing or symmetrization, in the form of relative difference to a reference spectrum ρ_{bulk} taken for the same single crystals after careful annealing, as given by the equation

$$\Delta=\frac{\rho-\rho_{bulk}}{\rho_{bulk}}. \tag{1}$$

With this presentation, the effect of positron trapping is immediately seen as the deviation of the Δ curve from the zero line.

If one assumes that the difference between ρ and ρ_{bulk} comes only from a fraction F of positrons trapped in vacancies, with a characteristic momentum distribution ρ_{vac}, Eq. (1) can be rewritten as

$$\Delta=F\frac{\rho_{vac}-\rho_{bulk}}{\rho_{bulk}}. \tag{2}$$

This equation tells that the shape of the Δ signal depends only on the morphology of the trap, whereas the intensity is proportional to F.

The experiment with deformed samples was carried out by using 5–9-purity polycrystalline Al; compression deformation was applied at room temperature up to 50% thickness reduction. The measurements were taken at LNT with the same procedure used for the quenched specimens. The results are shown in Fig. 1(b), once more in terms of relative difference to bulk [Eq. (1)].

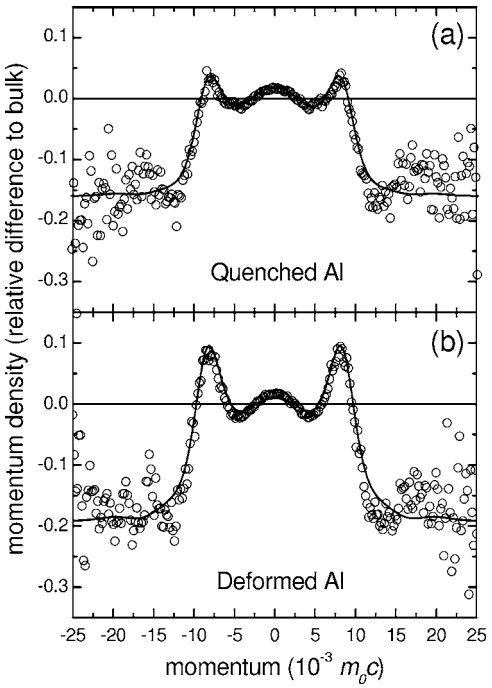

FIG. 1. CDB spectra for defected Al (relative differences to annealed Al). The solid line is the result of the *ab initio* LDA calculation (see text).

The comparison of Figs. 1(a) and 1(b) shows the following elements of similarity in the Δ curves: (a) a broad maximum centered at $p_x=0$; (b) a well-defined peak near to $p_x=8\times10^{-3}m_0c$; (c) a negative tail in the high-momentum region. The same elements can be found in previous CDB measurements for defected Al.[15,16] On the other hand, it may be noted that the curves of Figs. 1(a) and 1(b) cannot be scaled to a common master curve, as it would be predicted by Eq. (2) if the morphology of the traps were the same in quenched and in deformed Al.

This is clearly shown in Fig. 2, where the same ratios depicted in Fig. 1 are directly compared after vertical scaling (the statistical noise was reduced here by symmetrization and

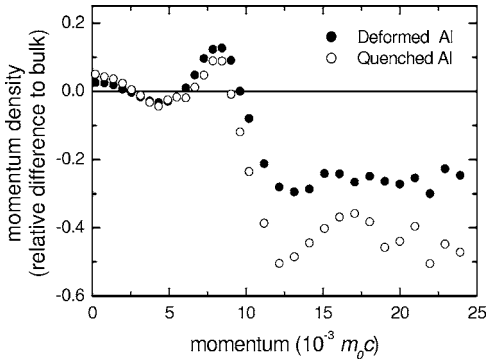

FIG. 2. CDB spectra for defected Al (relative differences to annealed Al), after scaling to 100% trapping.

TABLE I. Results of lifetime measurements at LNT. The last column gives the trapping fraction as determined by fitting the result of the LDA calculation to the experimental CDB data in Fig. 1.

Sample	τ_1 (ps)	τ_2 (ps)	I_2 (%)	F (%)[a]	F (%)[b]
Quenched Al	110±2	235±2	58±1.5	31±2	34
Deformed Al	57±2	225±2	86±1.5	64±2	64

[a]from lifetime data;
[b]from best-fit to momentum data

adjacent averaging). The chosen scaling factors (1/0.64 and 1/0.34, respectively for deformed and quenched Al data) are the reciprocals of the trapping fractions F; according to Eq. (2), the rescaled curves should be independent on the trapping fraction. The numerical values of F are best-fit values corresponding to the theoretical curves shown as solid lines in Figs. 1 and 2 (to be discussed in the next section). Ancillary positron lifetime measurements were performed in order to obtain an independent estimate of F. A standard fast-fast system with 250-ps resolution (FWHM of the prompt curve) was used. The data (about 6×10^6 counts per spectrum) were taken at LNT on freshly prepared samples; in spite of all possible care to reproduce every detail of the preparation procedure of the samples used for CDB measurements, minor differences in the defect densities are always possible. The spectra were analyzed in two exponential components (intensities I_1 and I_2, lifetimes τ_1 and τ_2) by the POSITRONFIT program.[17] The results are given in Table I, together with the trapping fraction F evaluated from the standard trapping model (STM) (Refs. 18 and 19) equation,

$$F = I_2\left(1-\frac{\tau_1}{\tau_2}\right). \tag{3}$$

It must be observed, however, that in the case of the deformed sample Eq. (3) must be taken as a lower limit, since the STM may not be entirely valid.[20]

III. THEORY

Ab initio calculations of the e^+-e^- momentum densities were performed for bulk Al and for various geometries of open-volume positron traps, with the aim of testing the possibility to reproduce the similarities and the differences mentioned at the end of the previous section and to isolate the physical mechanisms to which they are to be ascribed.

A general introduction to *ab initio* calculations of positron annihilation characteristics in solids can be found in Ref. 21. The procedure adopted in the present work was as follows. Valence electron densities were computed self-consistently in the framework of the local-density approximation (LDA) of the density-functional theory; the computation was carried out by employing the VASP code[22] with the projector augmented-wave (PAW) method[23] to account for the electron-ion core interaction. The PAW method enables plane-wave expansions for pseudovalence wave functions used in self-consistent calculations and the post-construction of all-electron valence wave functions resulting in accurate electron momentum densities.[24] In the calculations the Brillouin zone was sampled using a $3\times3\times3$ Monkhorst-Pack **k**-point mesh.[25] A cutoff of 241 eV was used when calculating the pseudovalence wave functions and a cutoff equivalent to $70\times10^{-3}m_0c$ was used when forming all-electron valence wave functions.

Using the total charge density from the VASP-PAW calculations and the LDA (Ref. 26) for electron-positron correlation potential, positron states were calculated on a three-dimensional real-space point grid.[27] The so-called "conventional scheme," in which the localized positron density does not affect the electron density, was used to describe trapped positrons. The annihilation rates of self-consistent all-electron valence states and atomic core electron states were calculated within the LDA (Ref. 26) for the electron-positron correlation. These partial annihilation rates were used as weighting factors when calculating momentum densities of annihilating electron-positron pairs within the so-called state-dependent enhancement scheme.[28,29] The momentum distributions corresponding to valence electrons were obtained by the three-dimensional Fourier transform on a cubic grid with the spacing of $0.67\times10^{-3}m_0c$ and those for the core electrons on a dense radial grid using parametrized forms of the positron wave function.[30]

A cubic supercell of 108 atomic sites in a periodic superlattice was used for the simulation of bulk and of defected Al. Vacancylike defects were simulated by empty atomic sites. The positions of the nearest neighbors of the missing atoms were moved from their normal lattice sites in order to reproduce the local relaxation in the proximity of the empty site. The explored range of possible relaxations was from 2% outward to 6% inward. Larger inward displacements are expected for the positron traps associated to dislocations, which can be essentially described as distorted vacancies with a reduced free volume.[31] The results presented below are only for isotropic relaxations. Simulations based on different hypotheses regarding the symmetry of the relaxation showed that changing the symmetry without changing the net amount of volume relaxation has negligible effects on positron lifetimes as well as on orientation-averaged one-dimensional momentum distributions. Computed one-dimensional momentum distributions for bulk and for defected Al were used for calculating the relative difference Δ by Eq. (2) (with $F=1$) after convolution with a Gaussian (FWHM $=3.5\times10^{-3}m_0c$) to simulate the experimental resolution.

The Δ curves in Fig. 3 correspond to different values of the linear relaxation at the empty site. After vertical scaling to account for a trapping fraction $F<1$, fair fits to the experimental CDB data shown in Fig. 1 can be obtained for outward relaxations between 1 and 0 % for the quenched sample and inward relaxations between 3 and 4 for the deformed sample. The curves for 0 and 4 % inward linear relaxation are shown in Fig. 1 and the corresponding best fit values for F are reported in the last column of Table I. The computed lifetimes are 234 and 211 ps, respectively, for 0 and 4 % inward relaxation; the measured lifetimes (235 and 225 ps) correspond to relaxations respectively near 0 and 2 % inwards. According to preliminary LDA computations,[27] the expected relaxation for an empty vacancy in bulk Al is 1.7 % inwards; when a positron is trapped into the vacancy,

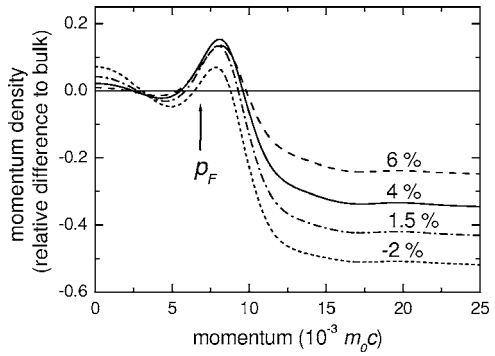

FIG. 3. Computed momentum densities (relative differences to bulk Al) for positron trapping at an empty site; labels on the curves show the isotropic inward relaxation of the nearest-neighbor positions (here, and in the following figures, negative values are conventionally attributed to outward relaxations). The Fermi momentum p_F is denoted by the upward arrow.

the relaxation is estimated at about 1.8 % outwards. No LDA prediction is available for vacancies stabilized by dislocations.

The simulation offers the possibility to isolate the different factors that contribute to build the characteristic shapes of the Δ curves. The following considerations can be made.

(i) The broad maximum at $p_x=0$ comes from the narrowing of the valence electron momentum distribution associated to the reduction of electron density at the defect. This effect is well known since the early studies of positron trapping at defects in metals,[7] but is clearly visible also in semiconductors.[8–11] The sensitivity of the effect to the size of the positron trap can be judged from Fig. 4, which shows the e^+-e^- momentum one-dimensional (1D) distribution including only the valence electron contribution; the curve for bulk Al is reported for comparison.

(ii) The negative value taken by Δ at high momentum is simply the result of the reduction of the core electron contribution to annihilation, which always occurs when the positron wave function becomes localized in an open-volume defect. The sensitivity of the effect to the local atomic arrangement is quantified in Fig. 5, where the ratio of core

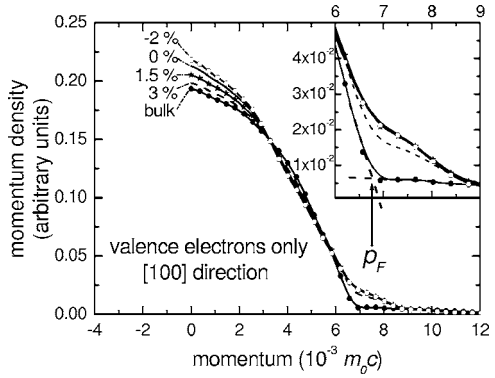

FIG. 4. Contribution of valence electrons to the e^+-e^- one-dimensional momentum density in bulk aluminum and in vacancylike defects with different inward linear relaxations (see labels). The Fermi momentum is denoted by the upward arrow.

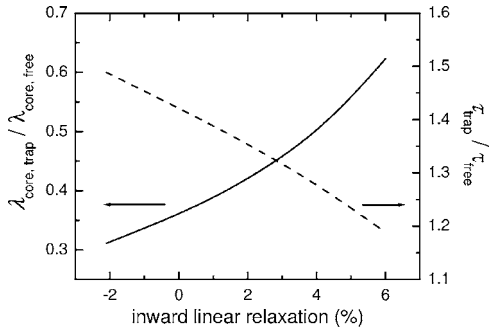

FIG. 5. Core annihilation rate (solid line, left vertical scale) and lifetime (dashed line, right vertical scale) for trapped positrons (relative to free positrons in bulk Al) vs the inward displacement of the nearest neighbors of the empty atomic site.

annihilation rate (ten core electrons/Al atom) for trapped positrons ($\lambda_{core,trap}$) to the corresponding core rate for bulk Al ($\lambda_{core,bulk}$) is plotted vs the relaxation degree. Figure 5 also shows the effect of the trap size on the positron lifetime. The predicted positron lifetimes for bulk Al is 165 ps.

(iii) The peak that is seen in Figs. 1(a) and 1(b) near $8\times10^{-3}m_0c$, i.e., just beyond the Fermi cutoff of the valence electron distribution, is due to the quantum confinement of the positron wave function in a region of atomic dimensions. The motion of the confined particle implies a non-negligible contribution to the total momentum carried away by the annihilation radiation. Figure 6 shows the one-dimensional momentum densities for positrons trapped at vacancylike defects with different degrees of relaxation. A visual gauge of the momentum scale of Fig. 6 is provided by a horizontal double-head arrow, which shows the minimum momentum indetermination that, by the uncertainty principle, corresponds to quantum confinement over a distance of 2 Å ($\frac{1}{2}$ of the lattice constant of bulk Al).

The momentum distributions of Fig. 6 are leptokurtic, i.e., more peaked than Gaussians. This gives some ambiguity in the definition of the width of the distributions. Figure 7 compares the simple prediction coming from the uncertainty principle ($\delta p_x=\hbar/\Delta x$, where Δx is $\frac{1}{2}$ of the relaxed cell edge)

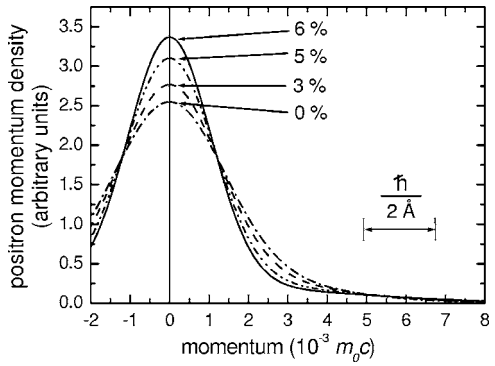

FIG. 6. One-dimensional momentum density for positrons trapped in vacancylike defects. The labels on the curves indicate the inward displacement of the nearest neighbors of the empty atomic site. The horizontal bar shows the expected momentum width for quantum confinement within 2.0 Å.

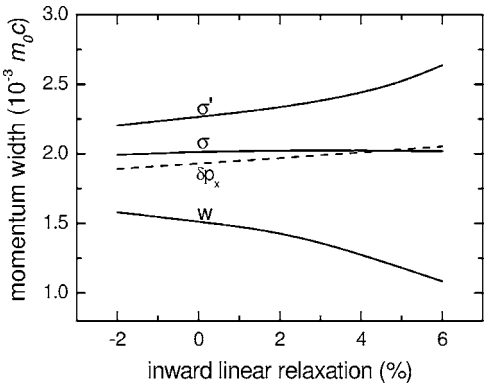

FIG. 7. Width of the positron momentum distribution vs inward linear relaxation. See text for the different definitions of the width parameters.

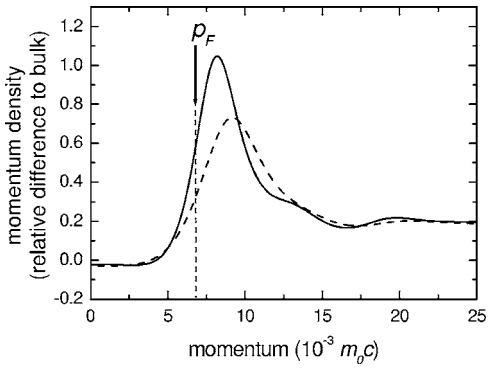

FIG. 8. Simulated effect of positron confinement in an unrelaxed vacancy on the relative difference of momentum densities. Solid line: resolution $2\times10^{-3}m_0c$; dashed line: resolution $4\times10^{-3}m_0c$. Fermi momentum: downward arrow.

with three different width parameters that would be coincident in the case of Gaussians:

$$\text{(a) } \sigma = (m_2)^{1/2},$$

where m_2 is the second central moment,

$$\text{(b) } \sigma' = \left(\frac{m_4}{3m_2^2}\right)^{1/4},$$

where m_4 is the fourth central moment,

$$\text{(c) } w = \frac{\text{HWHM}}{\sqrt{2\ln 2}},$$

where HWHM is the half width at half maximum.

The divergent behavior of σ' and w indicates increasing "peakedness" of the distributions with increasing inward relaxation. On the other hand, the standard deviation σ turns out to be almost constant within the explored range of relaxations; this result can be seen as a compensation of the reduction of trap size by the increased probability of finding the positron far from the center of the trap when the binding energy decreases.

The most relevant effect of positron motion is to smear the Fermi cutoff.[7,14] Since smearing enhances the counting rate beyond the Fermi cutoff (see inset in Fig. 4), additional counts fall in a region where the counting rate in the bulk metal reference spectrum is low, thus producing a peak in the ratio curves currently used for presenting CDB data. A convincing demonstration of the physical origin of the peak can be given by artificially reproducing the effect. The momentum contribution of a confined positron can be added to the electron momentum distribution without including any other effect of trapping (namely, reduction of the density of valence electrons at the vacancy and changes in the annihilation rates with different electron states). This is done by convoluting the momentum distribution calculated for bulk Al, where there is no effect of positron confinement, with the positron momentum distribution that is expected in case of trapping at a vacancylike defect (as depicted in Fig. 6). In any real experiment, the visibility of the effect depends on the resolution of the apparatus, which determines the more or less sharp definition of the Fermi cutoff. Figure 8 shows examples where the positron was assumed to be confined in an unrelaxed vacancy, and the hypothetical resolution (FWHM) was either $2\times10^{-3}m_0c$ (solid line) or $4\times10^{-3}m_0c$ (dashed line).

IV. CONCLUDING REMARKS

The experimental results presented in this work show a clear difference between CDB distributions taken for positrons trapped at quenched-in thermal vacancies or at dislocation-associated vacancylike defects. As the substantial difference between these species of trap is the extension of the open volume seen by the positron,[31] the observed effect gives a quantitative demonstration of the sensitivity of the CDB technique to the local geometry, which is additional to the well-known sensitivity to the local chemistry at the annihilation site.[4] The comparison of the experimental data with the theoretical prediction shows that the observed difference can be reproduced fairly well by assuming a linear relaxation of 3–4 % at the defect, i.e., a relative change of free volume near 10 % when passing from the quenched sample to the deformed sample. Differences of a comparable amount in the local geometry of the positron trap, which in pure metals can be produced by stress conditions, in an alloy may also come from decoration with solute elements. The message given by the present finding is that any modification of the defect geometry that affects the free volume is one factor that can never be overlooked when interpreting CDB measurements.

A second important factor to be taken into account in the case of CDB measurements in metallic systems is the smearing of the Fermi cutoff associated to the motion of confined positrons. When CDB data are presented in terms of ratio to the bulk momentum density, the smearing becomes manifested as a peak just beyond the bulk Fermi momentum. The visibility of the effect is enhanced when the smearing brings additional CDB counts in a region where the reference momentum distribution is low, thus the effect will be more evident for metals where the annihilation probability with core electrons is small. Aluminum is an example, and the effect is clearly seen also in Al alloys. In the case of alloys, when

CDB measurements are applied to the study of precipitation (for a review, see Ref. 6), the confinement peak can be a disturbance, as it is partially superimposed to the additional structures that are due to decoration of vacancylike defects by minority alloy components. This makes impossible to reproduce the CDB distribution for an alloy as a linear combination of the distributions measured for annealed samples of pure elements. An empirical attempt to circumvent the problem has been proposed by Somoza *et al.*,[16] who have obtained good fits of their experimental data for Al-Cu-based alloys by using linear combinations of distributions measured for defected samples of the alloy components. The present work encourages thinking that a better way to achieve the quantitative interpretation of CDB data can be the comparison with simulated momentum densities.

ACKNOWLEDGMENTS

The Italian authors acknowledge financial support by the Ministero dell'Istruzione, Università e Ricerca (Grant No. PRIN 2004–023079). The Finnish authors acknowledge financial support by the Academy of Finland through its Centre of Excellence Program (2000–2005).

[1] P. Hautojärvi, *Topics in Current Physics* (Springer, Heidelberg, 1979), Vol. 12.
[2] *Positron Solid-State Physics*, edited by W. Brandt and A. Dupasquier (North-Holland, Amsterdam, 1983).
[3] P. Hautojärvi, and C. Corbel, in *Positron Spectroscopy of Solids*, edited by A. Dupasquier and A. P. Mills, Jr. (IOS, Amsterdam, 1993).
[4] P. Asoka-Kumar, M. Alatalo, V. J. Ghosh, A. C. Kruseman, B. Nielsen, and K. G. Lynn, Phys. Rev. Lett. **77**, 2097 (1996).
[5] R. Krause-Rehberg and H. S. Leipner, *Positron Annihilation in Semiconductors* (Springer-Verlag, Berlin, 1999).
[6] A. Dupasquier, G. Kögel, and A. Somoza, Acta Mater. **52**, 4707 (2004).
[7] S. Berko and J. C. Erskine, Phys. Rev. Lett. **19**, 307 (1967).
[8] J. P. Peng, K. G. Lynn, M. T. Umlor, D. J. Keeble, and D. R. Harshman, Phys. Rev. B **50**, 11247 (1994).
[9] R. Ambigapathy, A. A. Manuel, P. Hautojärvi, K. Saarinen, and C. Corbel, Phys. Rev. B **50**, 2188 (1994).
[10] R. Ambigapathy, C. Corbel, P. Hautojärvi, A. A. Manuel, and K. Saarinen, J. Phys.: Condens. Matter **7**, L683 (1995).
[11] R. Ambigapathy, C. Corbel, P. Hautojärvi, A. A. Manuel, and K. Saarinen, Appl. Phys. A: Mater. Sci. Process. **62**, 529 (1996).
[12] M. Hasegawa, Z. Tang, T. Chiba, M. Saito, A. Kawasuso, T. Akahane, Z. Q. Li, Y. Kawazoe, and S. Yamaguchi, Mater. Sci. Forum **255**, 414 (1997).
[13] Z. Tang, M. Hasegawa, T. Chiba, M. Saito, A. Kawasuso, Z. Q. Li, R. T. Fu, T. Akahane, Y. Kawazoe, and S. Yamaguchi, Phys. Rev. Lett. **78**, 2236 (1997).
[14] M. A. Shulmann and S. Berko, *4th International Conference on Positron Annihilation*, Helsingør, 1976.
[15] K. G. Lynn, J. E. Dickman, W. L. Brown, M. F. Robbins, and E. Bonderup, Phys. Rev. B **20**, 3566 (1979).
[16] A. Somoza, M. P. Petkov, K. G. Lynn, and A. Dupasquier, Phys. Rev. B **65**, 094107 (2002).
[17] P. Kirkegaard, N. J. Pedersen, and M. Eldrup, *PATFIT–88 Program*, Risø National Laboratory, Report No. M-2740, 1989.
[18] W. Brandt, in *Positron Annihilation*, edited by A. T. Stewart and L. O. Roellig (Academic, New York, 1967), p. 178.
[19] D. C. Connors and R. N. West, Phys. Lett. **30A**, 24 (1969).
[20] G. Aldi, A. Dupasquier, U. La Malfa, S. Re Fiorentin, and C. Regazzoni, J. Phys. F: Met. Phys. **12**, 2185 (1982).
[21] M. J. Puska and R. M. Nieminen, Rev. Mod. Phys. **66**, 841 (1994).
[22] G. Kresse and D. Joubert, Phys. Rev. B **59**, 1758 (1999).
[23] P. E. Blöchl, Phys. Rev. B **50**, 17953 (1994).
[24] I. Makkonen, M. Hakala, and M. J. Puska, J. Phys. Chem. Solids **66**, 1128 (2005).
[25] H. J. Monkhorst and J. D. Pack, Phys. Rev. B **13**, 5188 (1976).
[26] E. Boronski and R. M. Nieminen, Phys. Rev. B **34**, 3820 (1986).
[27] I. Makkonen, M. Hakala, and M. J. Puska (unpublished).
[28] M. Alatalo, B. Barbiellini, M. Hakala, H. Kauppinen, T. Korhonen, M. J. Puska, K. Saarinen, P. Hautojärvi, and R. M. Nieminen, Phys. Rev. B **54**, 2397 (1996).
[29] B. Barbiellini, M. Hakala, M. J. Puska, R. M. Nieminen, and A. A. Manuel, Phys. Rev. B **56**, 7136 (1997).
[30] M. Alatalo, H. Kauppinen, K. Saarinen, M. J. Puska, J. Mäkinen, P. Hautojärvi, and R. M. Nieminen, Phys. Rev. B **51**, 4176 (1995).
[31] H. Häkkinen, S. Mäkinen, and M. Manninen, Phys. Rev. B **41**, 12441 (1990).